J Nanostruct Chem (2016) 6:309–327
DOI 10.1007/s40097-016-0204-3

ORIGINAL RESEARCH

Theoretical study of the adsorption of NO_x on TiO_2/MoS_2 nanocomposites: a comparison between undoped and N-doped nanocomposites

Amirali Abbasi[1,2,3] · **Jaber Jahanbin Sardroodi**[1,2,3]

Received: 31 July 2016 / Accepted: 20 September 2016 / Published online: 4 October 2016

Abstract First-principle calculations within density functional theory were performed to investigate the interactions of NO and NO_2 molecules with TiO_2/MoS_2 nanocomposites. Given the need to further comprehend the behavior of the NO_x molecules positioned between the TiO_2 nanoparticle and MoS_2 monolayer, we have geometrically optimized the complex systems consisting of the NO_x molecule oriented at appropriate positions between the nanoparticle and MoS_2 monolayer. The structural properties, such as bond lengths, bond angles, adsorption energies and Mulliken population analysis, and the electronic properties, including the density of states and molecular orbitals, were also analyzed in detail. The results indicate that the interactions between NO_x molecules and N-doped TiO_2 in TiO_2-N/MoS_2 nanocomposites are stronger than those between gas molecules and undoped TiO_2 in TiO_2/MoS_2 nanocomposites, which reveal that the N-doping helps to strengthen the interaction of toxic gas molecules with hybrid TiO_2/MoS_2 nanocomposites. The N-doped TiO_2/MoS_2 nanocomposites have higher sensing capabilities than the undoped ones, and the interaction of NO_x molecules with N-doped nanocomposites is more favorable in energy than the interaction with undoped nanocomposites. Therefore, the obtained results also present a theoretical basis for the potential application of TiO_2/MoS_2 nanocomposite as an extremely sensitive gas sensor for NO and NO_2 molecules.

Graphical Abstract

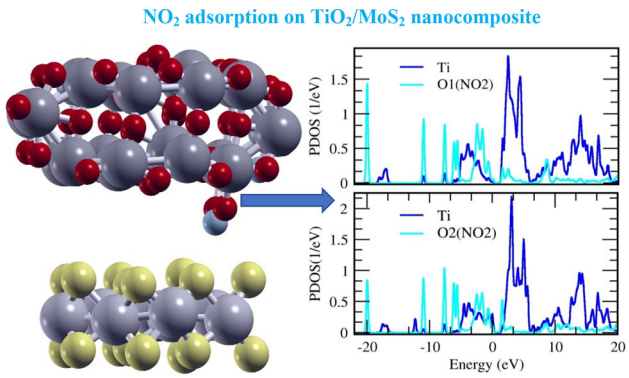

Keywords Density functional theory · NO_x · TiO_2/MoS_2 nanocomposite · Density of States · Adsorption

Introduction

Titanium dioxide (TiO_2, Titania) has aroused great attentions as an important semiconductor material due to its effectiveness and outstanding properties, such as non-toxicity, low cost, high catalytic efficiency, photoactivity [1], and stability. TiO_2 has been widely utilized in many fields, such as photo-catalysis, gas sensing, organic dye-

✉ Amirali Abbasi
a_abbasi@azaruniv.edu

[1] Molecular Simulation Laboratory (MSL), Azarbaijan Shahid Madani University, Tabriz, Iran

[2] Department of Chemistry, Faculty of Basic Sciences, Azarbaijan Shahid Madani University, Tabriz, Iran

[3] Computational Nanomaterials Research Group (CNRG), Azarbaijan Shahid Madani University, Tabriz, Iran

sensitized solar cells, water splitting, and pollutant degradation [2–5]. Three important polymorphs were found for TiO_2, namely, anatase, rutile, and brookite [6], in which anatase and rutile forms are the most widely studied ones in different fields of science and technology. The photocatalytic applications of TiO_2 were restricted due to its wide bandgap (3.2 eV), which allows the absorption of the solar spectrum at the ultraviolet region by a lower percentage (3–5 % of the incoming solar light). The doping of TiO_2 anatase with some nonmetal elements, such as nitrogen, is a convenient solution, which would enhance the photo-efficiency of TiO_2 to the visible region and improve its photocatalytic activity [7, 8]. Two-dimensional (2D) semiconductor

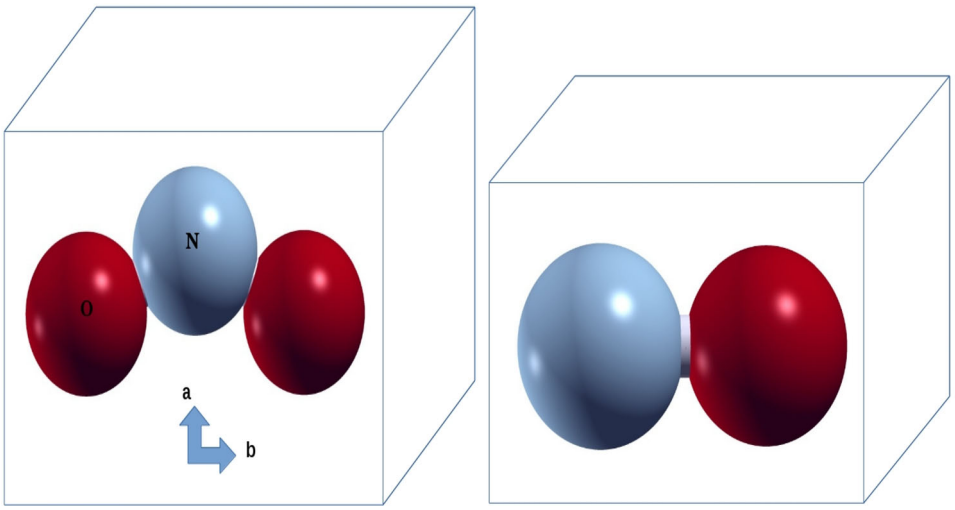

Fig. 1 Representation of NO and NO_2 molecules in a large cubic supercell

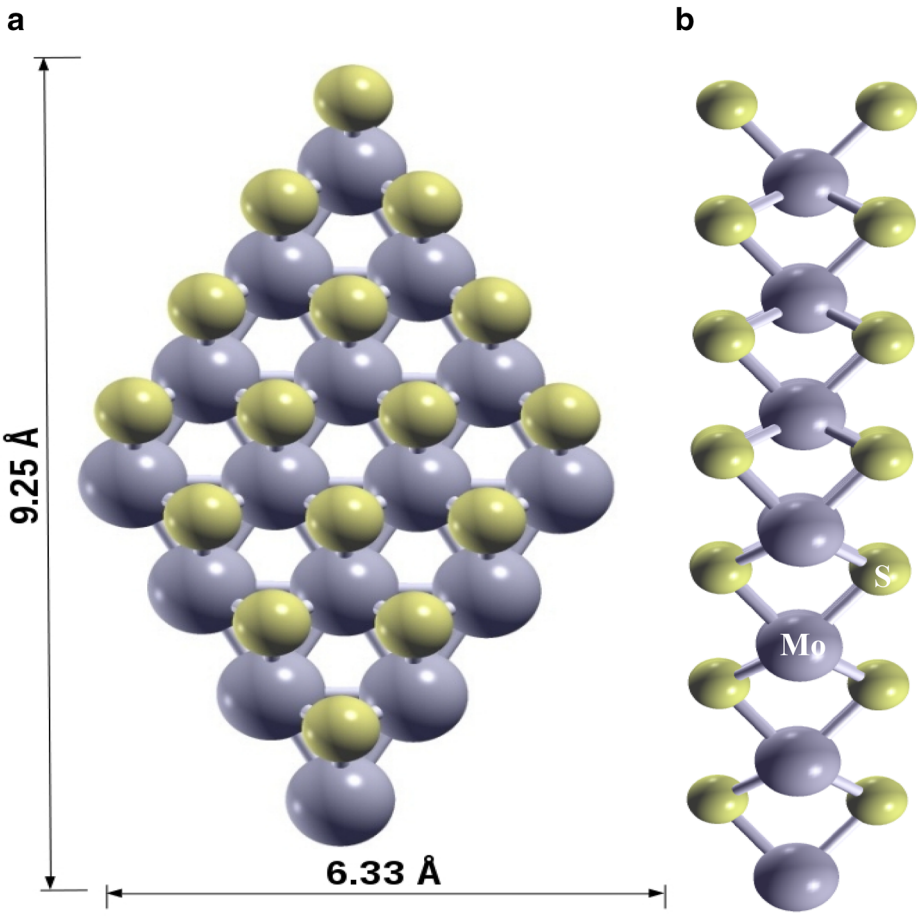

Fig. 2 Optimized structure of the chosen MoS_2 monolayer with area values, **a** front view and **b** lateral view. Mo atoms are sketched by *gray balls* and S atoms by *yellow balls*

materials, such as MoS_2 [9], and other dichalcogenides consisting of transition metals, such as $MoSe_2$, WS_2, and so on, indicate the final scale for chalcogenide dimension around the vertical direction. MoS_2, a layered structure consisting of Mo and S atoms arranged in hexagonal structure of atomic sheets of molybdenum and sulphur atoms, attracts numerous attentions due to the excellent electrical, mechanical, and optical properties, such as satisfied bandgap, thermal stability, carrier mobility, and so on [10–12]. MoS_2 has been broadly used in abundant applications, such as photocatalysts, nanotribology, lithium battery, dry lubrication, hydrodesulfurization catalyst, and photovoltaic cell because of its unique electronic, photosensitive, and catalytic properties [13–16]. Nanoelectronic devices fabricated on 2D materials, such as MoS_2, suggest also many efficiencies for these layered materials, which cause the further miniaturization of the integrated circuits beyond Moore's law. Recently, numerous electronic devices were made using the few-layer MoS_2 as an important component, such as field-effect transistors [17], sensors [18], etc. However, several computational studies of N-doped TiO_2 anatase nanoparticles and few-layer MoS_2 structures have been separately published, describing some of the main electronic and physical properties of these materials. Particularly, the gas-sensing capabilities of MoS_2-based field-effect transistors and sensing films for NO and NH_3 were experimentally revealed with an enhanced sensitivity in some other works [19, 20]. TiO_2/MoS_2 nanocomposites have been successfully synthesized for different purposes by some experimental methods [21–23]. There are no explanative computational studies on the adsorption behaviors of TiO_2/MoS_2 nanocomposites. NO_x molecules have been characterized as toxic gases which are mainly emitted from power plants and vehicle engines. For the general public, the most outstanding provenance of NO_2 is internal combustion engines that burn fossil fuels to work properly. In indoor places, NO_2 emission mainly stems from cigarette smoke, kerosene heaters, and stoves. Therefore, optimal removal of these harmful molecules is an important subject to human health and environmental protection [24]. In this study, the interaction of NO_x molecules with TiO_2/MoS_2 nanocomposites has been investigated by density functional theory (DFT) computations. We present here the results of calculations of complex systems consisting of NO_x molecule positioned between the TiO_2 anatase nanoparticle and MoS_2 monolayer. The electronic structure of the adsorption systems has also been analyzed, including the projected density of states (PDOSs) and molecular orbitals (MOs). The main aim of this study is to supply an overall understanding on the adsorption behaviors of nano-TiO_2/MoS_2 composites as highly sensitive NO_x sensors.

Computational details and structural models

Methodology

DFT calculations [25, 26] were performed as implemented in the Open-Source Package for Material eXplorer (OPENMX3.8) [27], being a well-organized software package for nano-scale materials simulations based on DFT, PAO basis functions, and VPS pseudopotentials [28, 29]. Pseudo-atomic orbitals were utilized as basis sets in the geometry optimizations. The considered cut-off energy is set to the value of 150 Rydberg in our calculations [29], The PAOs are generated via the basis sets (3-s, 3-p, and 1-d) for Ti atom, (3-s, 3-p, and 2-d) for Mo atom, (2-s and 2-p) for O and N atoms, (3-s and 3-p) for S atom with the chosen cut-off radii of 7 for Ti, 9 for Mo, 5 for O and N, and 8 for S (all in Bohrs). The generalized gradient approximation (GGA) of Perdew–Burke–Ernzerhof (PBE) was used to describe the exchange–correlation energy functional [30]. The convergence criterion of self-consistent field calculations was set at 1.0×10^{-6} Hartree, whereas that of energy calculation was chosen to be 1.0×10^{-4} Hartree/bohr. For the geometry optimization, 'Opt' is used as the geometry optimizer, which is a robust and efficient scheme. The crystalline and molecular structure visualization program, XCrysDen [31], was employed for displaying molecular orbital isosurfaces. The box considered in these computations contains 96 atoms (24 Ti, 48 O, 8 Mo, and 16 S atoms) of undoped or N-doped TiO_2 nanoparticle with MoS_2 monolayer. The Gaussian broadening method for evaluating electronic DOS is used. For NO_x adsorption on the TiO_2/MoS_2 nanocomposite, the adsorption energy is computed via the following formula:

$$\Delta E_{ad} = E_{(composite+adsorbate)} - E_{composite} - E_{adsorbate} \quad (1)$$

where $E_{(composite\ +\ adsorbate)}$ is the total energy of the adsorption system, $E_{composite}$ is the energy of the TiO_2/MoS_2 nanocomposite, and $E_{adsorbate}$ represents the energy of non-adsorbed NO_x molecules. Based on this relation, the most stable configurations would have negative adsorption energies. A higher adsorption energy corresponds to a stronger adsorption between host and adsorbed molecule.

Model building

NO and NO_2 molecule model

The chemical formulae of nitric oxide and nitrogen dioxide molecules are NO and NO_2. NO has linear structure, while

NO_2 represents a bent geometrical structure. The structures of NO and NO_2 molecules were represented in Fig. 1. Distances and angles of the considered molecules were computed in a large cubic supercell. The calculated N–O bond length of free NO molecule is 1.16 Å, while for the bent structure of NO_2 molecule, the bond length and bond angles were calculated to be 1.20 Å and 134°, respectively. All these computed values are in comprehensive agreement with the computational results and the experimentally reported data [32].

MoS_2 model

Molybdenum disulfide (MoS_2) is a layered structure containing molybdenum transition metal, which belongs to the family of two-dimensional dichalcogenides. A hexagonally arrangement of atomic sheets of MoS_2 containing Mo and S atoms set as an S–Mo–S sandwich forms MoS_2 monolayer. The monolayer of MoS_2 model studied here contains 24 atoms in total (8 Mo and 16 S atoms). MoS_2 structure is relaxed for calculating the optimized structural parameters. The calculated S–Mo bond length, Mo–Mo distance, and S–S distance in monolayer are 2.43, 3.20, and 3.15 Å, respectively. These computed bond lengths are somewhat consistent with the values of bulk material [33], in reasonable agreement with the reported data [34, 35]. However, there are negligible discrepancies between the results of MoS_2 and its bulk material, which can be ignored. The area of the MoS_2 slab is 9.25 Å × 6.33 Å. The optimized structure of MoS_2 model was displayed in Fig. 2.

TiO_2 anatase model

A 3 × 2 × 1 supercell of TiO_2 anatase along x, y, and z directions was utilized for constructing the considered TiO_2

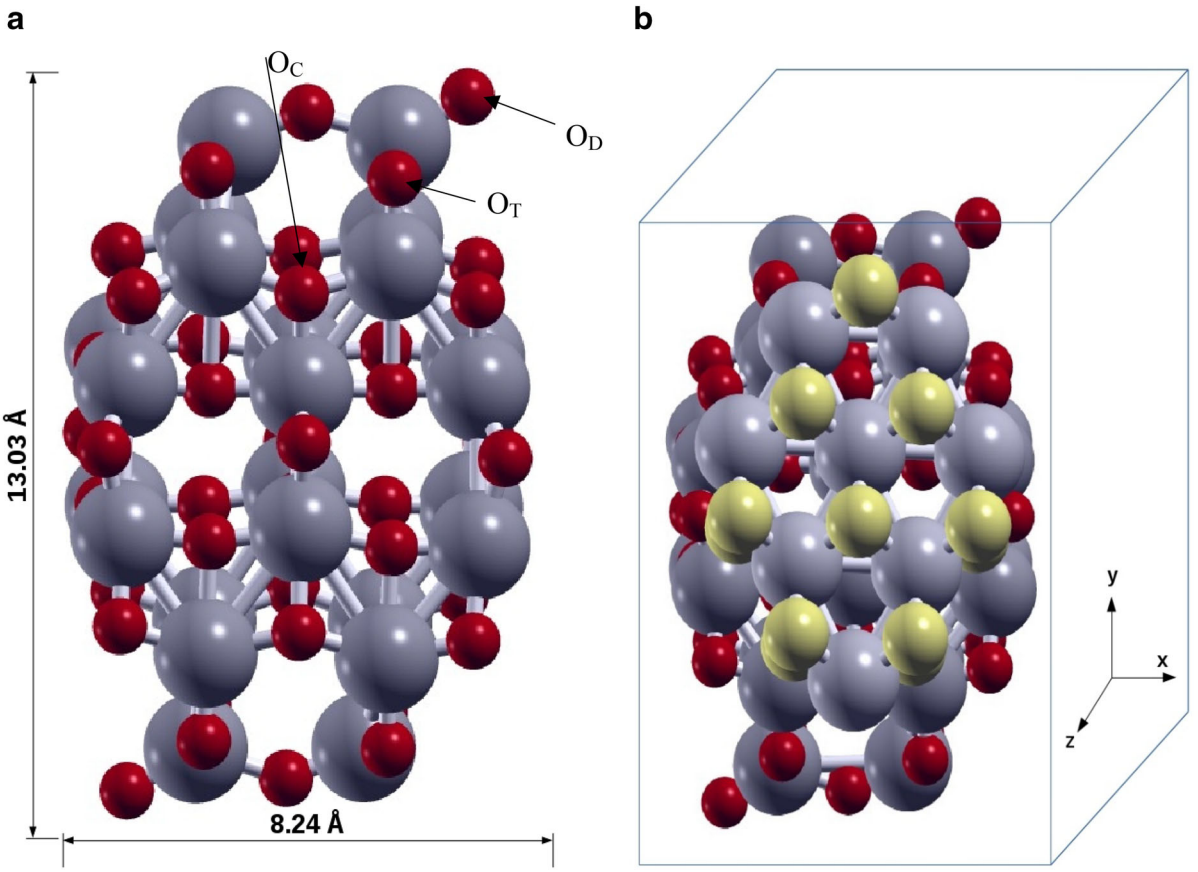

Fig. 3 Optimized structures of **a** undoped 72 atom TiO_2 anatase nanoparticle constructed using the 3 × 2 × 1 unit cells (O_C: central oxygen; O_T: twofold coordinated oxygen; O_D: dangling oxygen) and **b** TiO_2/MoS_2 nanocomposite constructed from TiO_2 nanoparticle and MoS_2 monolayer. Ti atoms are sketched by *dark gray balls*, O atoms by *red balls* and N atoms by *blue balls*

anatase nanoparticles containing 72 atoms. The unit cell is available at "American Mineralogists Database" webpage [36] and was reported by Wyckoff [37]. Two appropriate oxygen atoms of TiO_2 nanoparticle were replaced by nitrogen atoms to model the N-doped particles. Doping of TiO_2 nanoparticle with nitrogen atom is done according to two doping positions. These two doping positions refer to the middle oxygen and twofold coordinated oxygen atoms substitutions illustrated by O_C and O_T in Fig. 3a, respectively. The area of the anatase nanoparticle is 13.03 Å × 8.24 Å. The crystalline structure of TiO_2 contains two kinds of titanium atoms, namely, fivefold coordinated titanium (5f-Ti) and sixfold coordinated one (6f-Ti), and two kinds of oxygen atoms, namely, threefold coordinated oxygen (3f-O) and twofold coordinated one (2f-O) atoms (see Fig. 3a). [38] It was found that the twofold coordinated oxygen and fivefold coordinated titanium atoms are more reactive than the threefold coordinated oxygen and sixfold coordinated titanium atoms due to the undercoordination in twofold coordinated oxygen and fivefold coordinated titanium atoms. The thickness of the vacuum spacing is 11.5 Å, which is helpful to avoid the additional interactions between the neighbor particles. The optimized structure of TiO_2/MoS_2 nanocomposite was displayed in Fig. 3b. Figure 4 also displays the optimized geometries of the N-doped TiO_2/MoS_2 nanocomposites. The results of geometrical optimizations represent that the O_T-substituted TiO_2/MoS_2 nanocomposite is more favorable in energy than the O_C-substituted one.

Results and discussion

Bond lengths, bond angles, and adsorption energies

NO interacts with TiO_2/MoS_2 nanocomposites

For NO molecule, three adsorption configurations are studied here, including the adsorption configurations of types A, B, and C, as shown in Fig. 5. The calculated adsorption energy values for NO_x molecule adsorbed on the considered nanocomposites have been listed in Table 1.

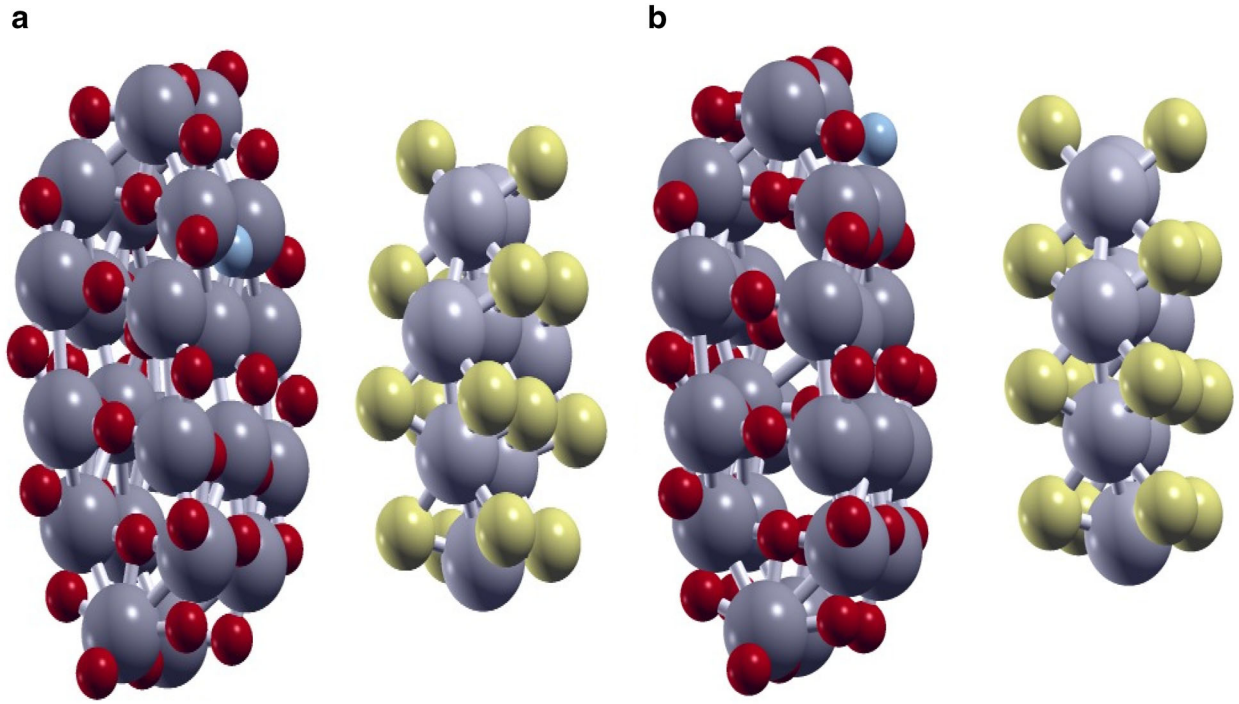

Fig. 4 Optimized geometries of two types of N-doped TiO_2/MoS_2 nanocomposites. **a** O_C-substituted nanocomposite, which refers to substitution of a threefold coordinated oxygen atom and **b** O_T-substituted nanocomposite, representing the substitution of a twofold coordinated oxygen atom

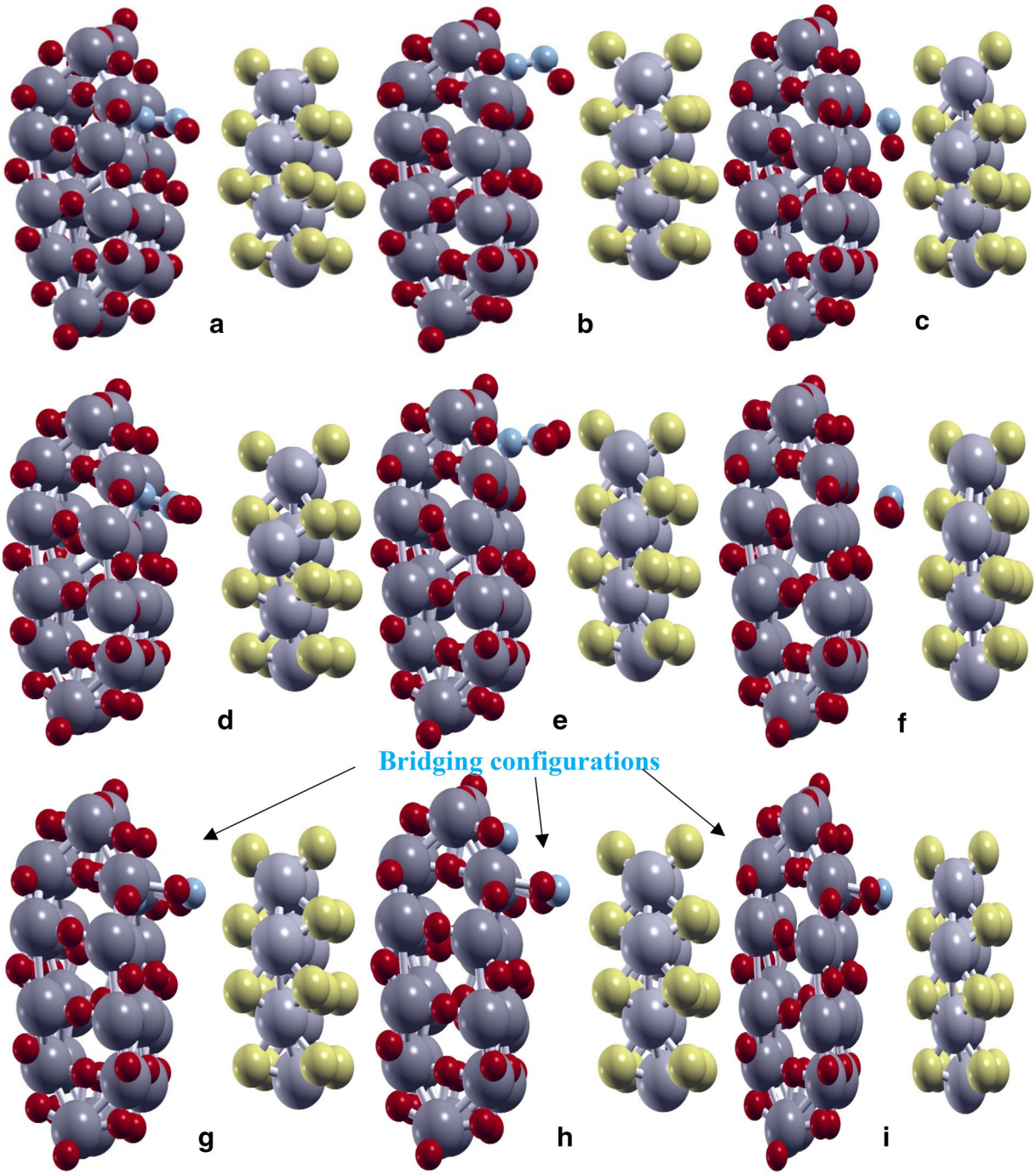

Fig. 5 Optimized geometry configurations of the interaction of NO and NO_2 molecules with TiO_2/MoS_2 nanocomposites. The NO molecule is preferentially adsorbed on the doped nitrogen site of TiO_2 nanoparticle, whereas NO_2 is adsorbed on both the doped nitrogen atom and fivefold coordinated titanium atoms. Configurations *A–C* represent the interaction of nanocomposites with NO molecules and the configurations *D–I* show the interaction between nanocomposites and NO_2 molecules

Table 1 Bond lengths (in Å), Mulliken charges, and adsorption energies (in eV) for NO_x molecule adsorbed on TiO_2/MoS_2 nanocomposites

Bond Composite	N–O_1 bond length	N–O_2 bond length	New N–N bond length	Average Ti–N length	New N–O bond length	Mulliken charge	Adsorption energy
NO adsorption							
Non-adsorbed	1.16	–	–	1.84 1.94	–	−0.122	−2.18
a	1.23		1.63	2.12	–		
b	1.30	–	1.43	1.99	–	−0.066	−3.01
c	1.19	–	–	–	3.16	−0.269	−0.50
NO_2 adsorption							
Non-adsorbed	1.20	1.20	–	1.84 1.94			
d	1.31	1.30	1.45	2.18		−0.064	−1.43
e	1.30	1.30	1.48	2.01		−0.107	−2.12
f	1.28	1.28	–	–	2.50	−0.014	−0.22

Table 2 Bond lengths (in Å), angles (in degrees), Mulliken charges, and adsorption energies (in eV) for complexes providing two contacting point between NO_2 molecule TiO_2/MoS_2 nanocomposites

Composite	New Ti–O1 bond length	New Ti–O2 bond length	N–O1 bond length	N–O2 bond length	O–N–O bond angle	Mulliken charge	Adsorption energy
g	2.41	2.53	1.28	1.29	122.3	−0.101	−1.42
h	2.03	2.28	1.30	1.36	117.4	0.180	−2.22
i	2.14	2.36	1.30	1.34	120.6	0.145	−0.92

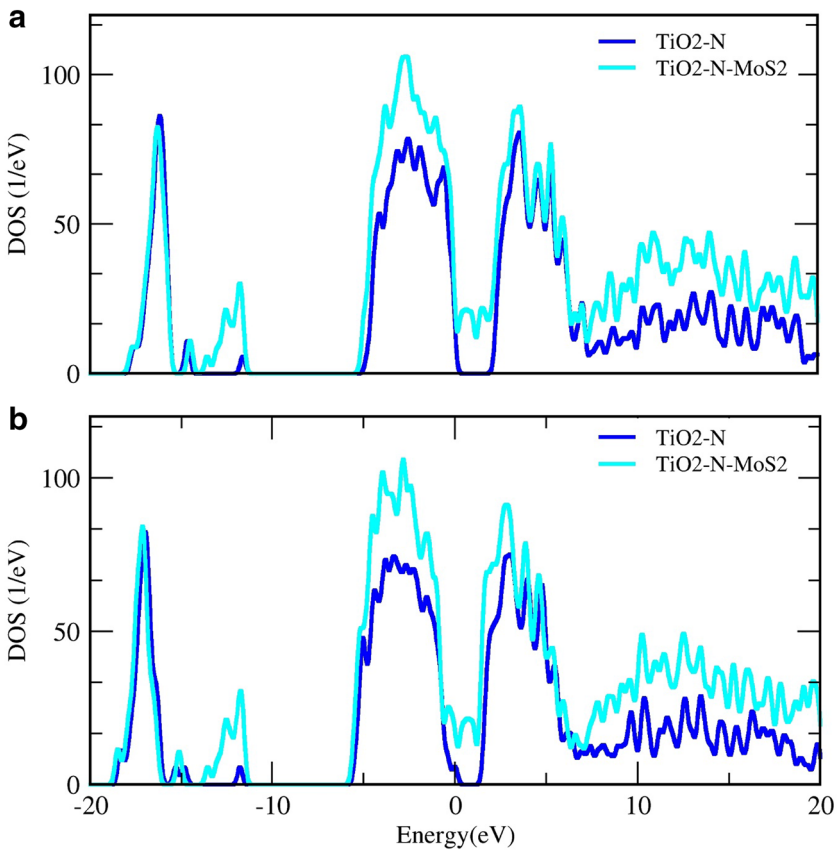

Fig. 6 Total density of states for N-doped TiO_2 and two types of N-doped TiO_2/MoS_2 nanocomposites. **a** O_C-substituted nanocomposite and **b** O_T-substituted one

This figure presents the orientations of NO molecule towards the N-doped TiO_2/MoS_2 nanocomposites. For instance, complex A was made from the TiO_2/MoS_2 nanocomposite with O_C-substituted TiO_2 nanoparticle and NO molecule with nearly downward oxygen. NO can stably adsorb on N-doped TiO_2/MoS_2 nanocomposite, compared to the adsorption on the undoped one. The nitrogen atom of NO molecule is preferentially attracted to the doped nitrogen atom of nanocomposite, resulting in the formation of chemical bond between these two nitrogen atoms. The adsorption energy of the NO molecule on the N-doped TiO_2/MoS_2 nanocomposite (composite A or B) is much higher than that of undoped TiO_2/MoS_2 nanocomposite, which reveals that NO molecule has a stronger interaction with N-doped nanocomposite than with undoped one. These results also indicate that the interaction of NO molecules with N-doped TiO_2/MoS_2 nanocomposites is more energetically favorable than the interaction of NO with undoped nanocomposites. This implies that the N-doped nanocomposite adsorbs NO molecule more effectively compared to the undoped one. Besides this, the configuration B is the most

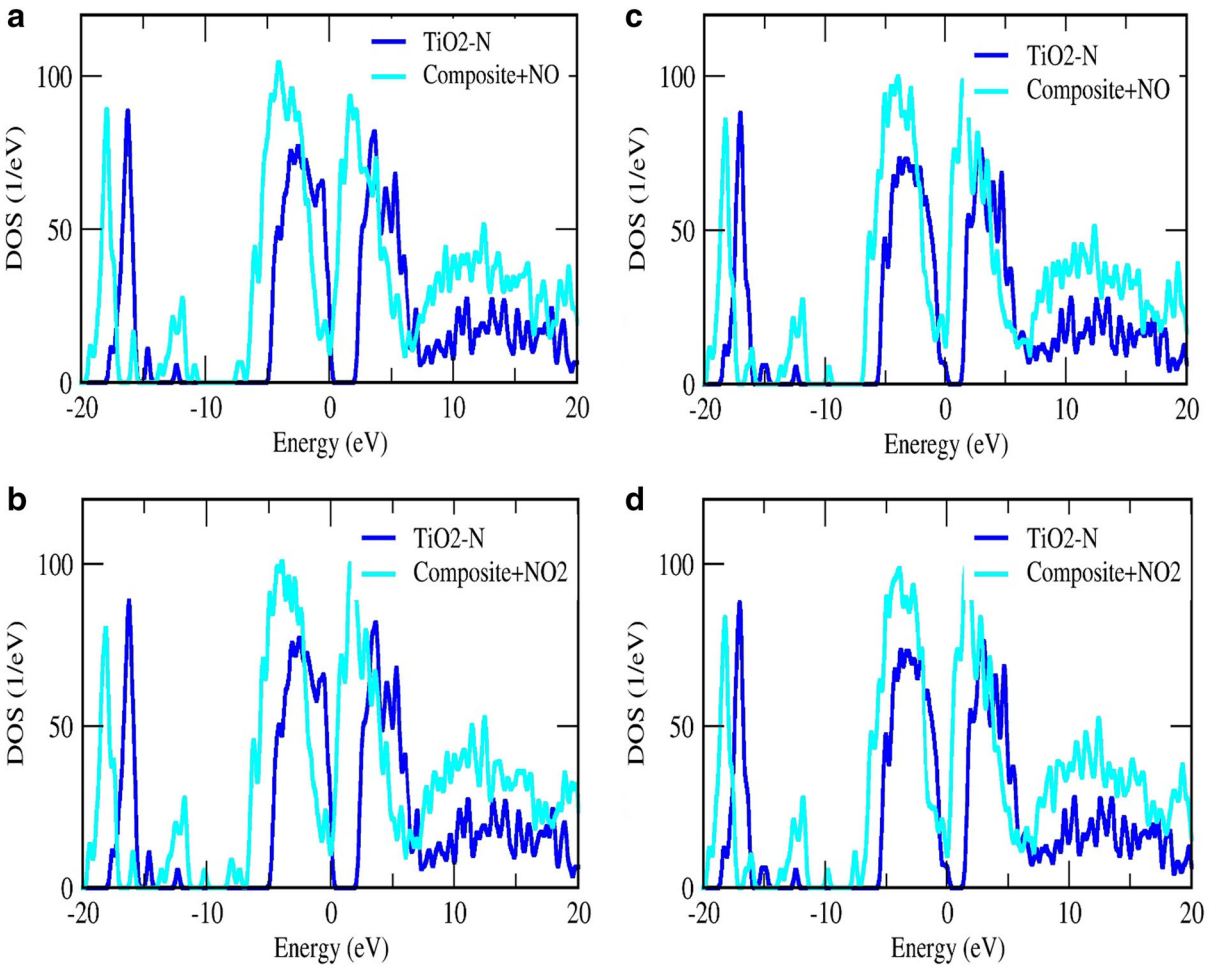

Fig. 7 DOS for the different adsorption configurations of the NO_x molecule on the considered TiO_2/MoS_2 nanocomposites, **a** A complex (NO molecule adsorbed on the O_C-substituted nanocomposite); **b** D complex (NO_2 molecule adsorbed on the O_C-substituted nanocomposite); **c** B complex (NO molecule adsorbed on the O_T-substituted nanocomposite); **d** E complex (NO_2 molecule adsorbed on the O_T-substituted nanocomposite)

stable configuration compared to the configuration A due to its more negative adsorption energy. Configuration B contains O_T-substituted nanocomposite with adsorbed NO molecule. The adsorption energy of this configuration is more negative than that of other configurations, which suggests that the adsorption of NO molecule on the O_T-substituted nanocomposite is more energy favorable than the adsorption on the O_C-substituted one (see Table 1). Since a greater value of adsorption energy gives rise to a strong interaction between adsorbate and the adsorbent, it can be seen that there is a stronger interaction between NO and N-doped nanocomposite compared to NO and undoped nanocomposite, implying the dominant effect of N-doping. It means that the nitrogen doping strengthens the interaction of NO with TiO_2/MoS_2 nanocomposites. The greater the adsorption energy, the higher tendency for adsorption, and, therefore, more efficient adsorption. Table 1 summarizes the bond length values before and after the adsorption of NO molecule on the nanocomposites. The bond lengths given in this table are included N–O bonds of NO_x molecule, average Ti–N distance, and new N–N and N–O distances between the nanocomposite and adsorbed NOx molecule. The values reported in this table show that the Ti–N bonds and N–O bond of the adsorbed NO molecule are elongated, because the electronic density transfers from the Ti–N bonds of N-doped TiO_2 and N–O bond of the adsorbed NO molecule to the newly formed N–N and N–O distances between the nanocomposite and molecule. This transfer of electronic density indicates that the N–O bond of NO molecule is weakened after the adsorption.

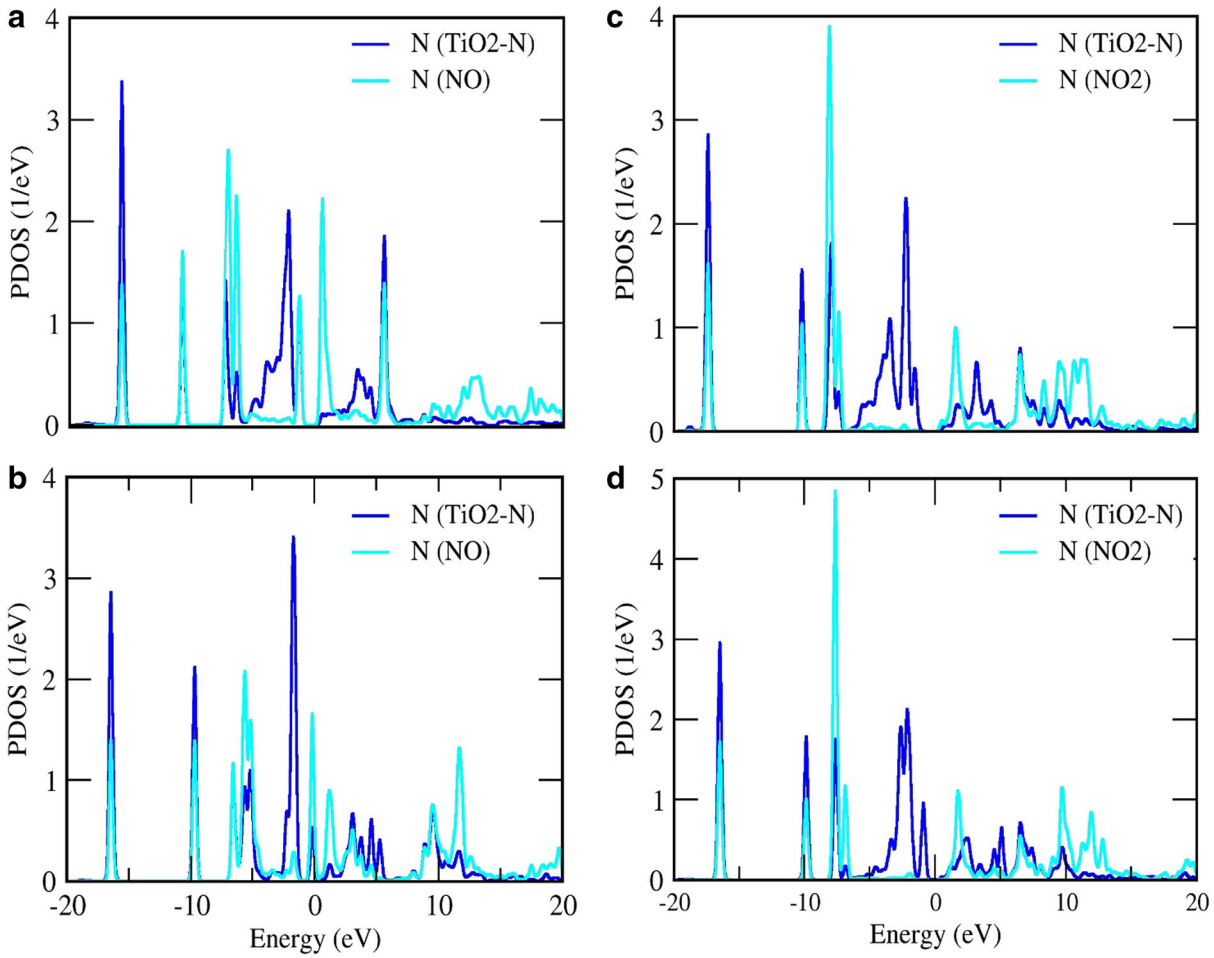

Fig. 8 PDOS for the interaction of NO_x molecule with TiO_2/MoS_2 nanocomposites, **a** A complex; **b** B complex; **c** D complex; **d** E complex

NO_2 interacts with TiO_2/MoS_2 nanocomposites

The interaction of NO_2 molecule with the substituted nitrogen atom of TiO_2/MoS_2 nanocomposites has also been displayed in Fig. 5 as specified by types D-F adsorption geometries. For the doped nitrogen site, the adsorption process is expected to be more energy favorable than that on the dangling oxygen atom site. The reason can be simply sought using the data collected in Table 1. Similarly, the NO_2 molecule preferentially interacts with the doped nitrogen site on the nanoparticle surface, in comparison with the other surface oxygen atoms. Table 1 also lists the lengths for Ti–N bonds and N–O bonds of the adsorbed NO_2 molecule and the newly formed N–N and N–O distances. The results of this table indicate that the Ti–N bonds of the nanocomposite and the N–O bonds of the NO_2 molecule are stretched after NO_2 adsorption. Because the electronic density transfers from the Ti–N bonds and N–O bonds to the newly formed distances between the nanocomposite and

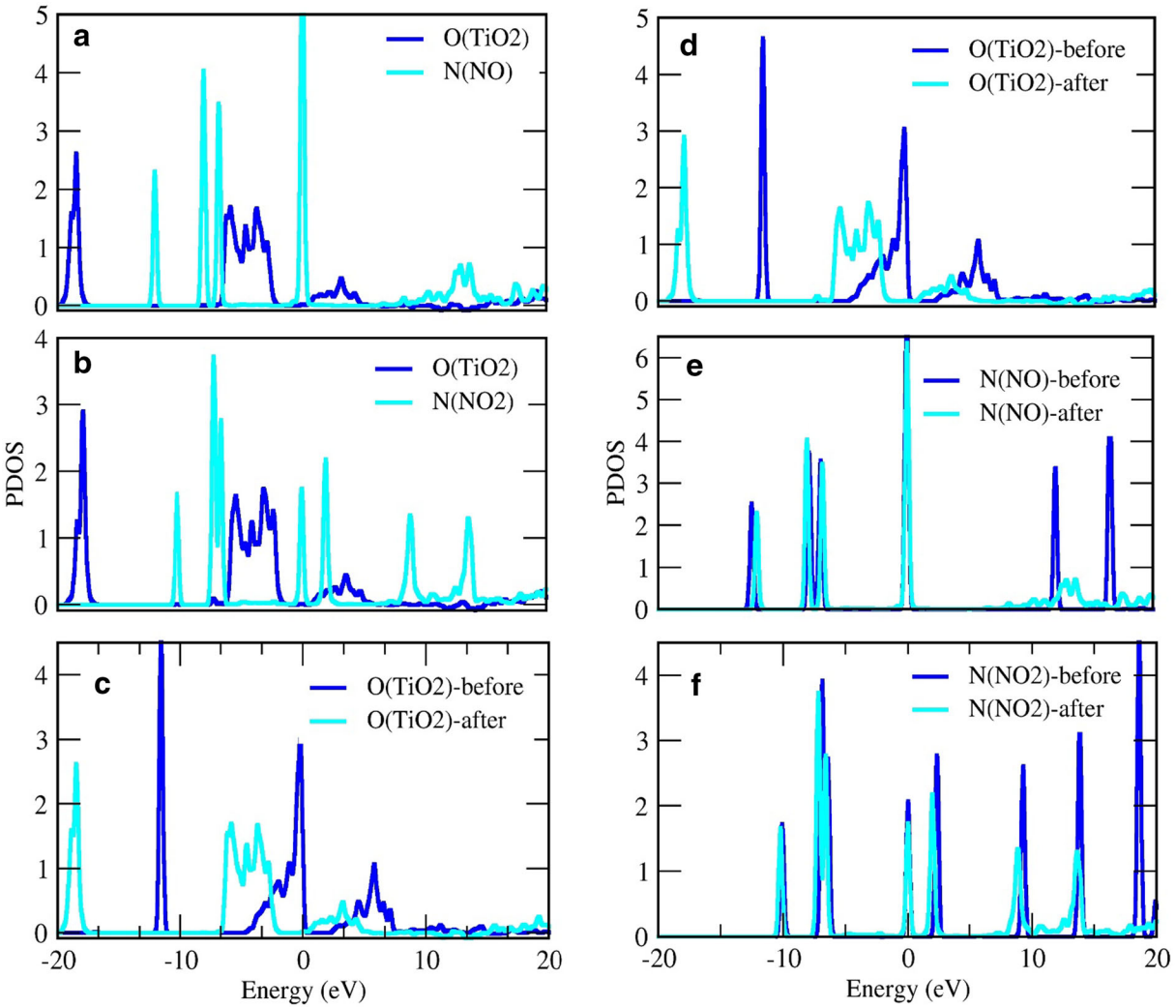

Fig. 9 PDOS for the interaction of NO_x molecule with TiO_2/MoS_2 nanocomposites, **a** C complex (NO molecule adsorbed on the pristine nanocomposite); **b** F complex (NO_2 molecule adsorbed on the pristine nanocomposite); **c** C complex; **d** F complex; **e** C complex; **f** F complex

adsorbed NO_2 molecule. In configuration D, the nitrogen atom in the NO_2 molecule interacts with the doped nitrogen site on the TiO_2 nanoparticle to form a strong chemical bond and, therefore, strong interaction (1.45 Å N–N bond length). Among three models for NO adsorption, the adsorption configuration in which the nitrogen atom of NO interacts with the doped nitrogen site of TiO_2 at O_T position is the most energy favorable one. In the case of NO_2 adsorption, the adsorption energy of configuration E is much higher (more negative) than that of configuration D and undoped system adsorption (configuration F). It should be noted that the adsorption on the O_T-substituted nanocomposite leads to the stable configurations (stronger interactions), compared to the adsorptions on the O_C-substituted one. As can be seen from Tables 1 and 2, the adsorption energies on the O_T-substituted nanocomposites (complexes E and H) are more negative than the adsorption energies on the O_C-substituted ones, implying that NO_2 adsorption on the O_T-substituted nanocomposites is energetically more favorable than the adsorption on the O_C-substituted ones. As a result, the adsorption of NO_2 molecule on the N-doped TiO_2/MoS_2 nanocomposite is more energy favorable than the adsorption of NO_2 on the undoped nanocomposite, indicating that the N-doped nanocomposite can adsorb NO_2 molecule more efficiently. Thus, the N-doping

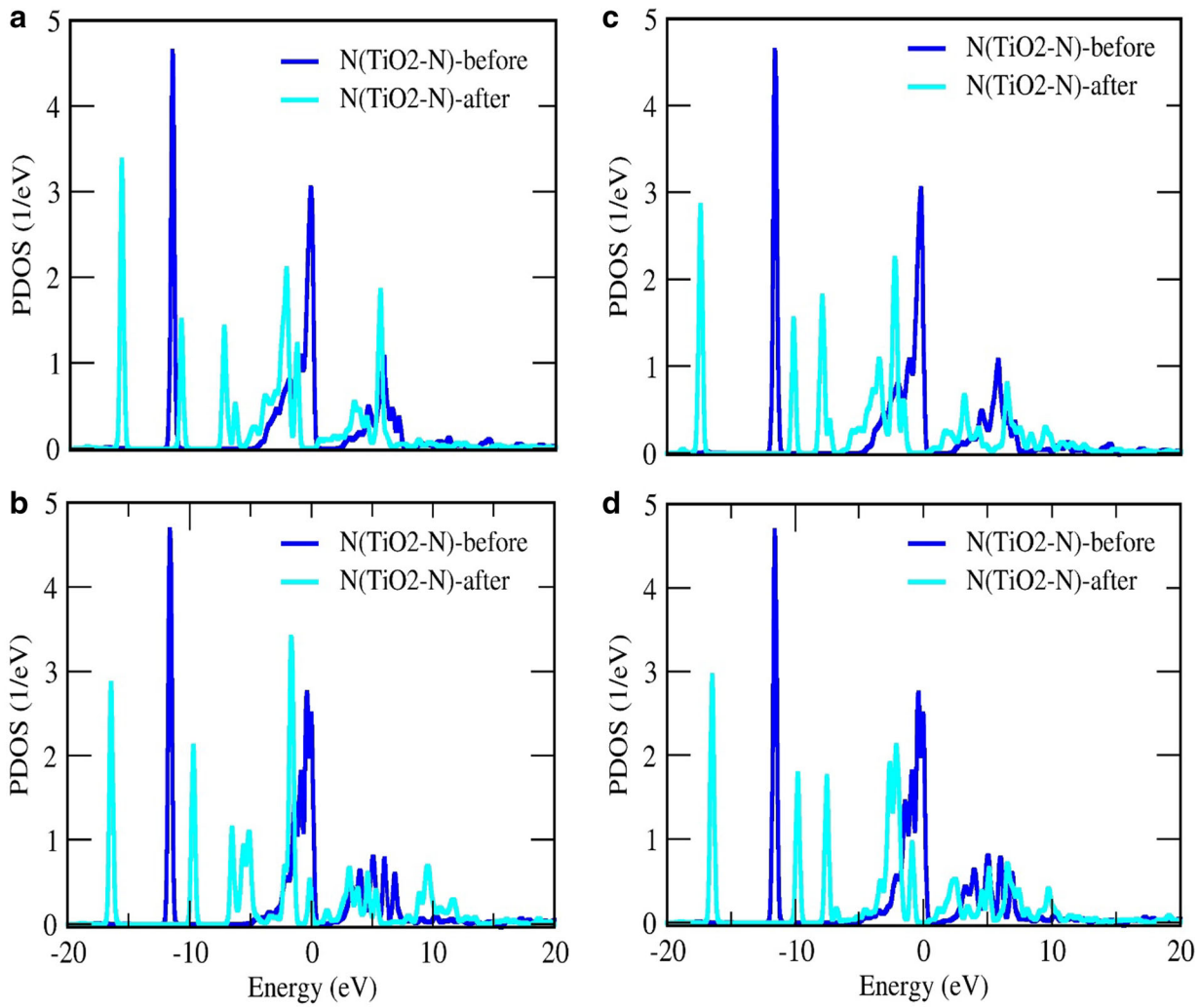

Fig. 10 PDOS of the nitrogen atom of nanocomposite before and after the adsorption process, **a** A complex; **b** B complex; **c** D complex; **d** E complex

strengthens the interaction of NO_2 molecule with TiO_2/MoS_2 nanocomposites. The O–N–O bond angles of the NO_2 molecule have been decreased after the adsorption process because of the formation of new chemical bond between nitrogen atom of NO_2 with nitrogen atom of TiO_2 nanoparticle. This chemical bond formation leads to an increase in the p characteristics of bonding molecular orbitals. Thus, the *sp* hybridization of nitrogen in the NO_2 molecule converts to near-sp^3 hybridization. For the case of TiO_2 adsorption on the fivefold coordinated titanium site presenting two contacting point between the nanoparticle and NO_2 molecule, the bond length and bond angle values have been reported in Table 2. We can see two newly formed Ti–O bonds between the titanium atoms of the nanoparticle with oxygen atoms of NO_2 molecule. This adsorption configuration is referred to as bridge configuration, and their complexes were illustrated in Fig. 5 (G–I complexes). The N–O bonds of NO_2 molecule have been lengthened after the adsorption process, suggesting the weakening of the N–O bonds. In addition, the adsorption process results in a decrease in the O–N–O bond angle values of NO_2. The adsorption energy analysis reveals that the complex H is the most energy favorable complex in comparison with complex G and both are more stable than the pristine system adsorption. These results show that the NO_x adsorption on

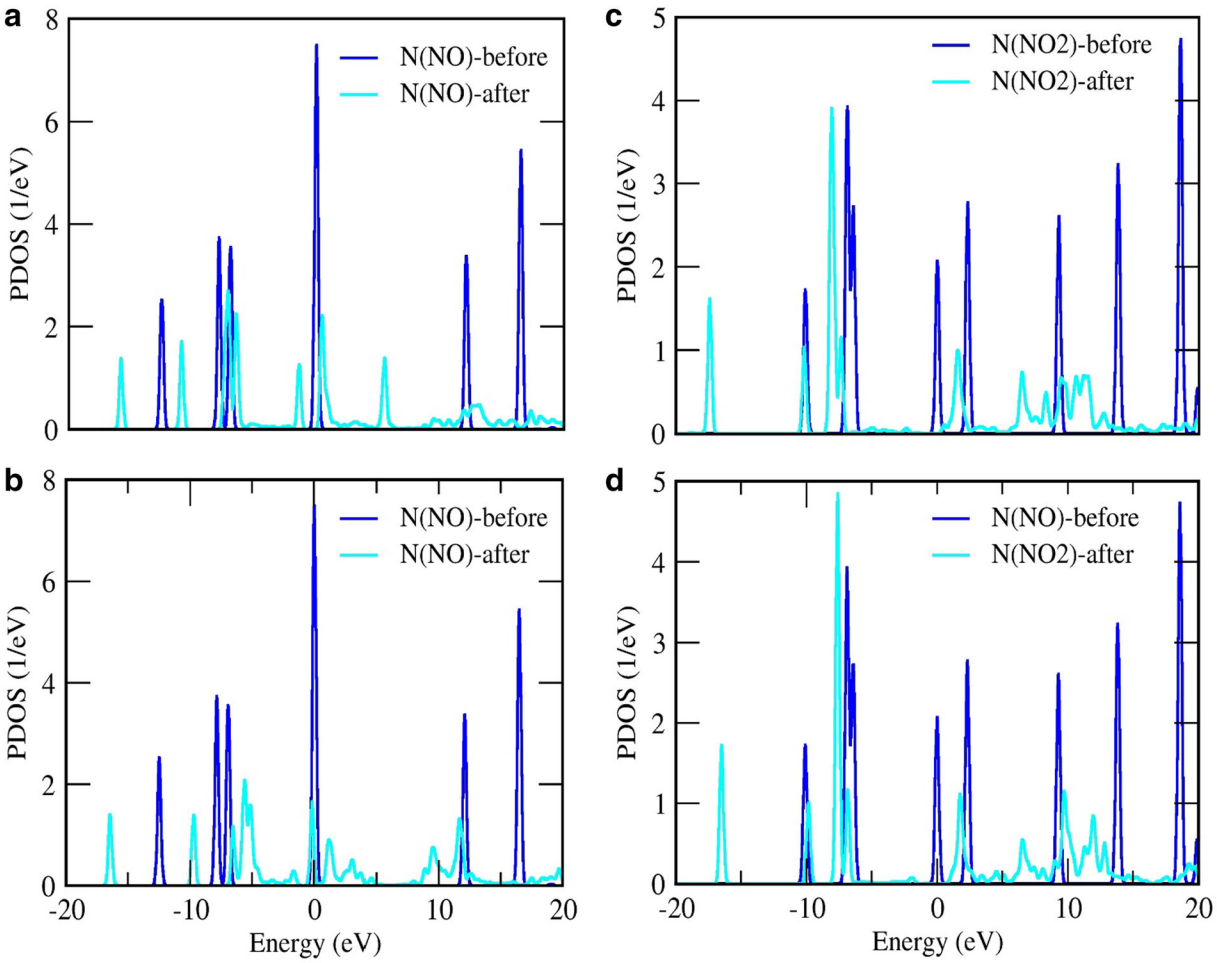

Fig. 11 PDOS of the nitrogen atom of NOx molecule before and after the adsorption process, **a** A complex; **b** B complex; **c** D complex; **d** E complex

the N-doped nanocomposite is more favorable in energy than the NO_x adsorption on the pristine nanocomposite. By considering this, we found that the nitrogen doping strengthens the interaction of NO_x molecule with TiO_2/MoS_2 nanocomposites. The obtained improvements on the structural and electronic properties of TiO_2/MoS_2 nanocomposites here represent that the N-doped TiO_2-based nanocomposite can be efficiently utilized in the removal and sensing of toxic NO_x molecule.

Electronic structures

Figure 6 presents the total density of states (TDOS) for N-doped TiO_2 anatase nanoparticles and corresponding TiO_2/MoS_2 nanocomposites. This figure reveals a creation of small peak in the density of states (DOSs) of N-doped nanocomposite at the energy ranges near to -12 eV. TDOSs of adsorption configurations were also displayed in Fig. 7. A closer inspection of these figures indicates the increase of the discrepancies between DOS of N-doped TiO_2 and nanocomposite by adding the MoS_2 monolayer and adsorption of NO_x. These differences included considerable shifts in the energies of the peaks and appearance of some peaks in the DOS of the studied systems. As distinct from these figures, the DOSs of the considered nanocomposites were mainly shifted to the lower energy values after the adsorption process. Therefore, the resultant variations in the energy of the

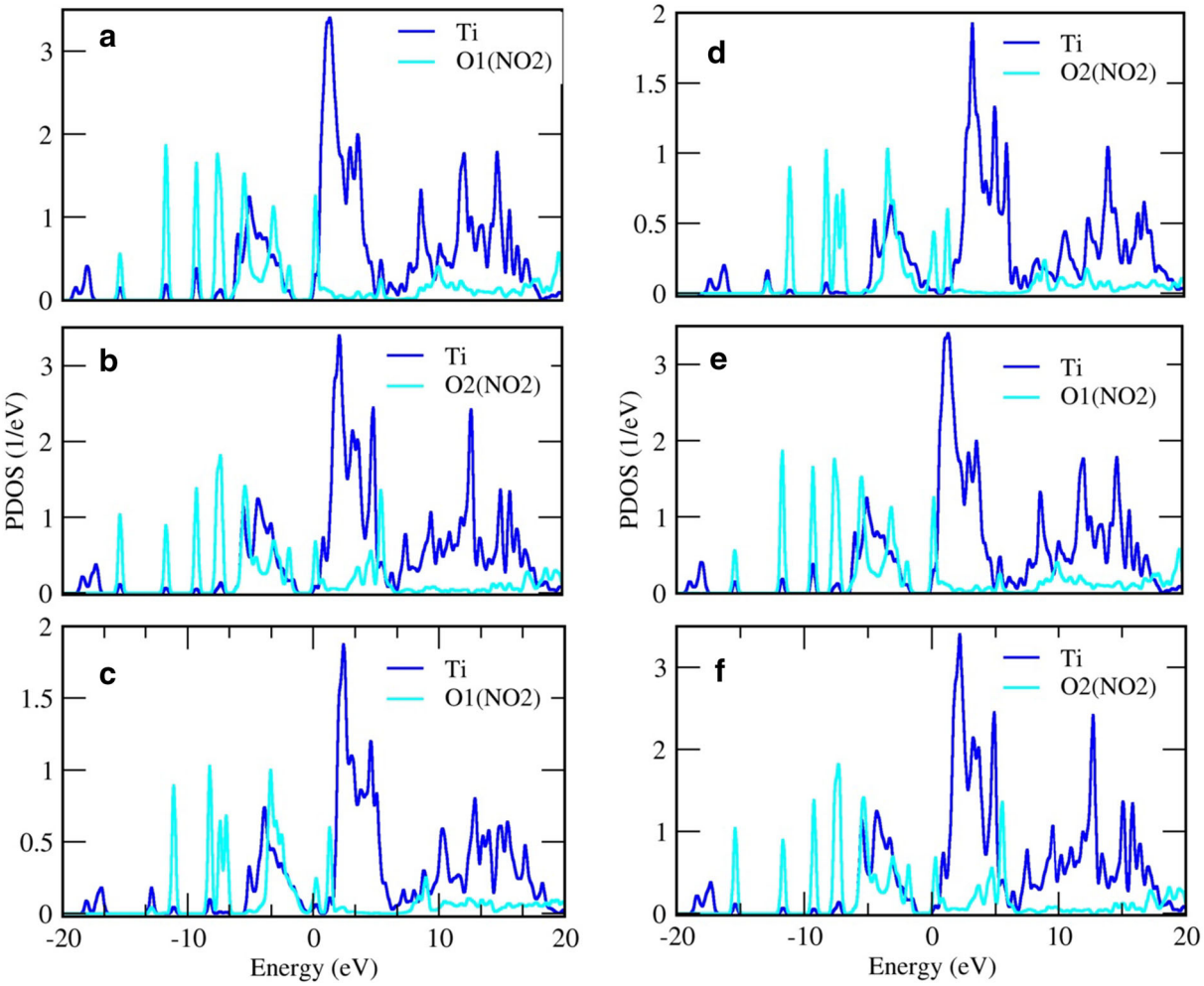

Fig. 12 PDOS of the titanium and oxygen atoms in complexes providing two contacting point between the nanocomposite and adsorbed molecule, **a** G complex (NO_2 adsorbed on the O_C-substituted nanocomposite in a bridge geometry); **b** G complex; **c** H complex (NO_2 adsorbed on the O_T-substituted nanocomposite in a bridge geometry); **d** H complex; **e** I complex (NO_2 adsorbed on the pristine nanocomposite in a bridge geometry); **f** I complex

states can have positive effects on the electronic transport properties of the nanocomposites and in turn can provide a helpful procedure for designing and engineering NO_x sensors based on N-doped TiO_2 and two-dimensional transition metal dichalcogenides (i.e., MoS_2 monolayer). The projected partial density of states (PDOSs) for the interaction of NO_x molecule with TiO_2/MoS_2 nanocomposites have been displayed in Fig. 8a–d. Panels (a, b) present the PDOS of the nitrogen atom of NO molecule and the doped nitrogen atom of N-doped nanocomposite. The large overlap between the PDOS of the mentioned atoms exhibits that the nitrogen atom of NO molecule interacts with the doped nitrogen atom of nanocomposite, suggesting the formation of new N–N bond. The PDOSs for NO_2 adsorption on the doped nitrogen site have also been shown as panels (c, d), which indicate a high overlap between the PDOS of nitrogen atom of NO_2 molecule and the nitrogen atom of nanocomposite and consequently forming a chemical bond. For NO and NO_2 adsorption on the middle oxygen (O_C site), the calculated PDOSs have been displayed in Fig. 9 (panels a, b), representing a low PDOS overlap between the nitrogen atom of NO and NO_2 molecules and the O_C atom of nanocomposite. This means a weak interaction between NO_x and nanocomposite. The other panels of Fig. 9 represent the PDOS of oxygen atom of nanocomposite before and after the adsorption on the undoped nanocomposite, as well as the PDOS of nitrogen atoms of NO and NO_2 molecules. As can be seen, the main difference is the creation a small peak in the PDOS curves and also shifting the position of the peaks to the lower lying energies. Figure 10a–d shows the PDOS of the nitrogen atom of nanocomposite before and after the adsorption on the N-doped nanocomposite, which also suggests a shifting of the PDOS of nitrogen atom to the lower energy values. To further discover the

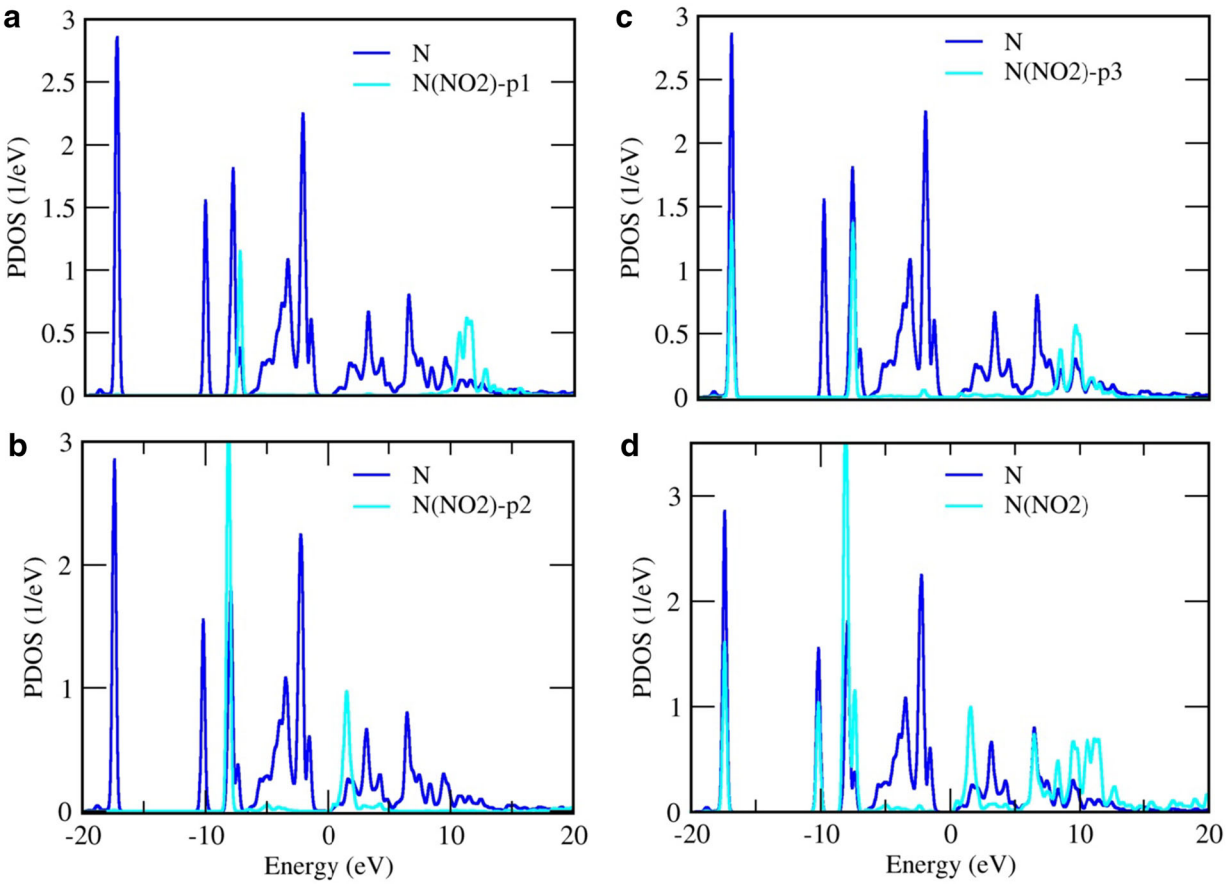

Fig. 13 PDOS of the nitrogen atoms and their related p orbitals after the adsorption process for D complex

electronic variations at the adsorption site, the PDOSs of nitrogen atom of NO and NO_2 molecule before and after the adsorption were also presented in Fig. 11a–d. Similarly, it can be seen from these PDOS plots that the biggest difference is the creation of some small peaks and also the state changing to the smaller energy values. The PDOSs of the complexes providing two contacting point (G, H and I) have also been displayed in Fig. 12, which indicate a higher overlap between the PDOS of Titanium atoms with two left and right oxygen atoms in all six panels. This means a formation of two chemical bonds between the titanium and oxygen atoms. Figures 13 and 14 represent the PDOSs of nitrogen atoms and their related p orbitals for complex D. As can be seen from these figures, p^3 orbital of the nitrogen atom of nanocomposite and NO_2 represents a considerable overlap with the other atom participating in chemical bond formation. This is an indication of the higher contribution of p^3 orbital in chemical bond in comparison with the other orbitals. The PDOSs of nitrogen atoms and their p orbitals for complex E have also been displayed in Fig. 15, indicating a high overlap between the PDOS of nitrogen atom with p^1 atomic orbital compared to the other orbitals. The HOMO and LUMO molecular orbitals were also displayed in Figs. 16 and 17, respectively. A closer inspection reveals that the HOMOs are strongly located on the nanoparticle, whereas the electronic densities in the LUMOs are mainly dominant on the NO_x molecules. As can be seen from Fig. 17, the electronic density in the LUMOs seems to be distributed over the NO_x molecules and on the middle of newly formed bonds. The accumulation of the electronic density at the middle of the newly formed bonds confirms the formation of new bonds and consequently the transfer of electronic density from the Ti–N bonds and N–O bonds to the newly formed bonds.

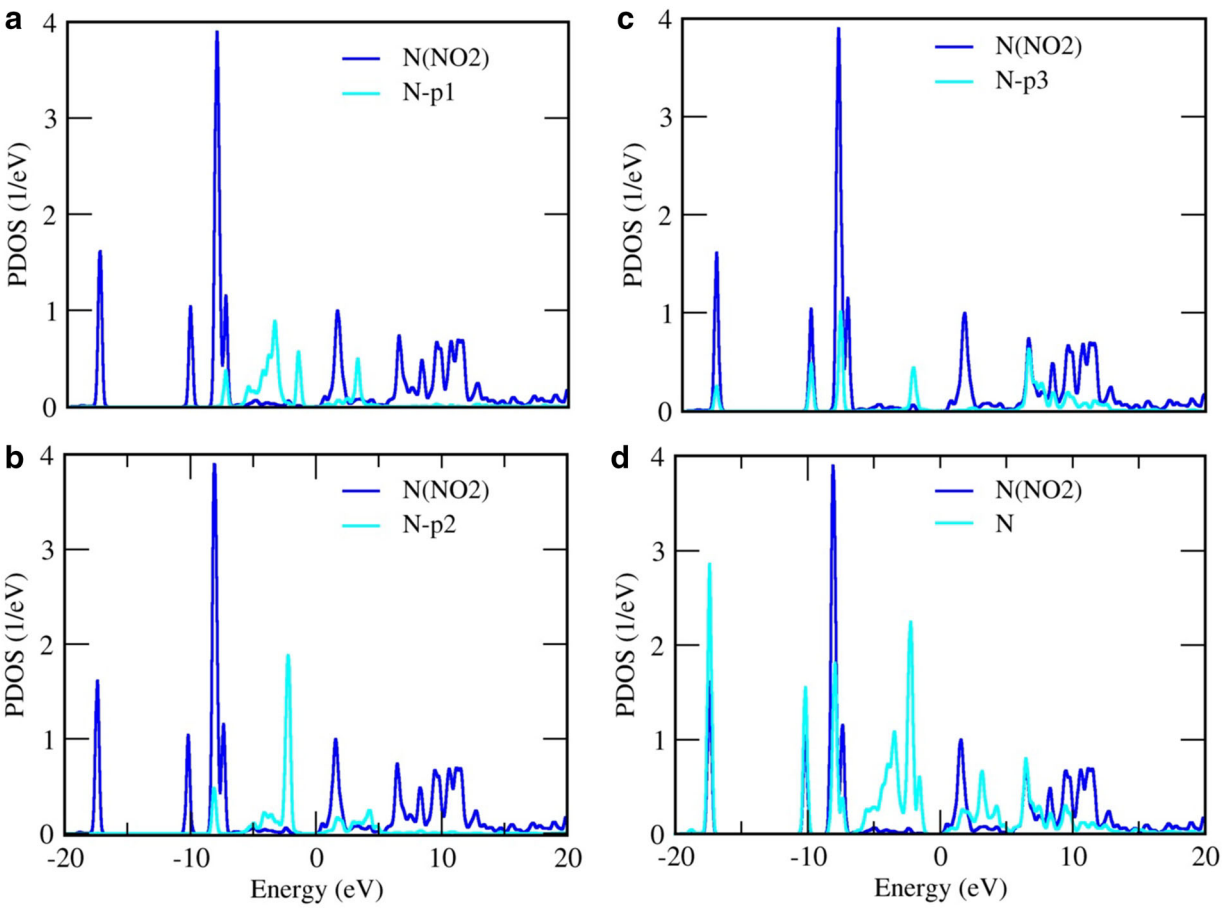

Fig. 14 PDOS of the nitrogen atoms and their related p orbitals after the adsorption process for D complex

However, the resultant improvements on the electronic properties of TiO_2/MoS_2 nanocomposites obtained by N-doping here demonstrate that the N-doped TiO_2/MoS_2 nanocomposites have stronger sensing capabilities than the pristine ones. To fully analyze the NO_x adsorption on the considered TiO_2/MoS_2 nanocomposites, the Mulliken population analysis has been conducted to analyze the charge distribution of the atoms and bonds in a complex system. The calculated Mulliken charge values for studied complexes were collected in Tables 1 and 2. For complex A, NO_x adsorption induces a considerable charge transfer of about −0.122 e from NO_x molecule to the nanoparticle, suggesting that NO_x acts as an acceptor. In other words, the NO_x molecule receives electros from nanocomposite. This leads to the changes in the conductivity of the system, which would be an efficient property to aid in the design and fabrication of novel sensor devices for nitrogen oxides recognition.

Conclusions

DFT calculations were conducted to investigate the interaction of NO_x molecules with undoped and N-doped TiO_2/MoS_2 nanocomposites to effectively understand the sensing properties of these nanocomposites in adsorption processes. The bond angles of the adsorbed NO_2 molecule are decreased compared to those in the isolated gas phase NO_2, which lead to an increase in the p characteristics of bonding molecular orbitals of nitrogen in the NO_2 molecule. The

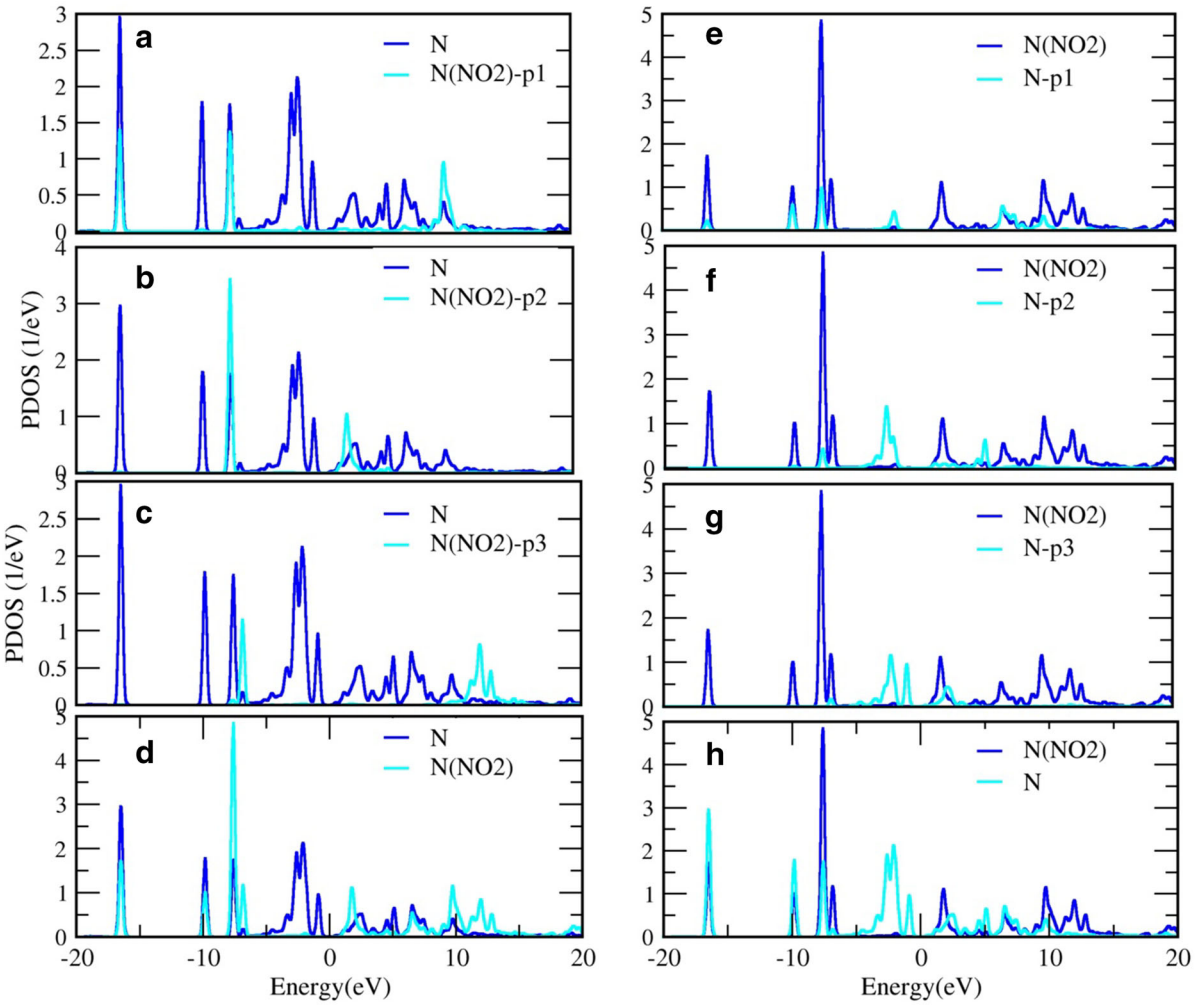

Fig. 15 PDOS of the nitrogen atoms and their related p orbitals after the adsorption process for E complex

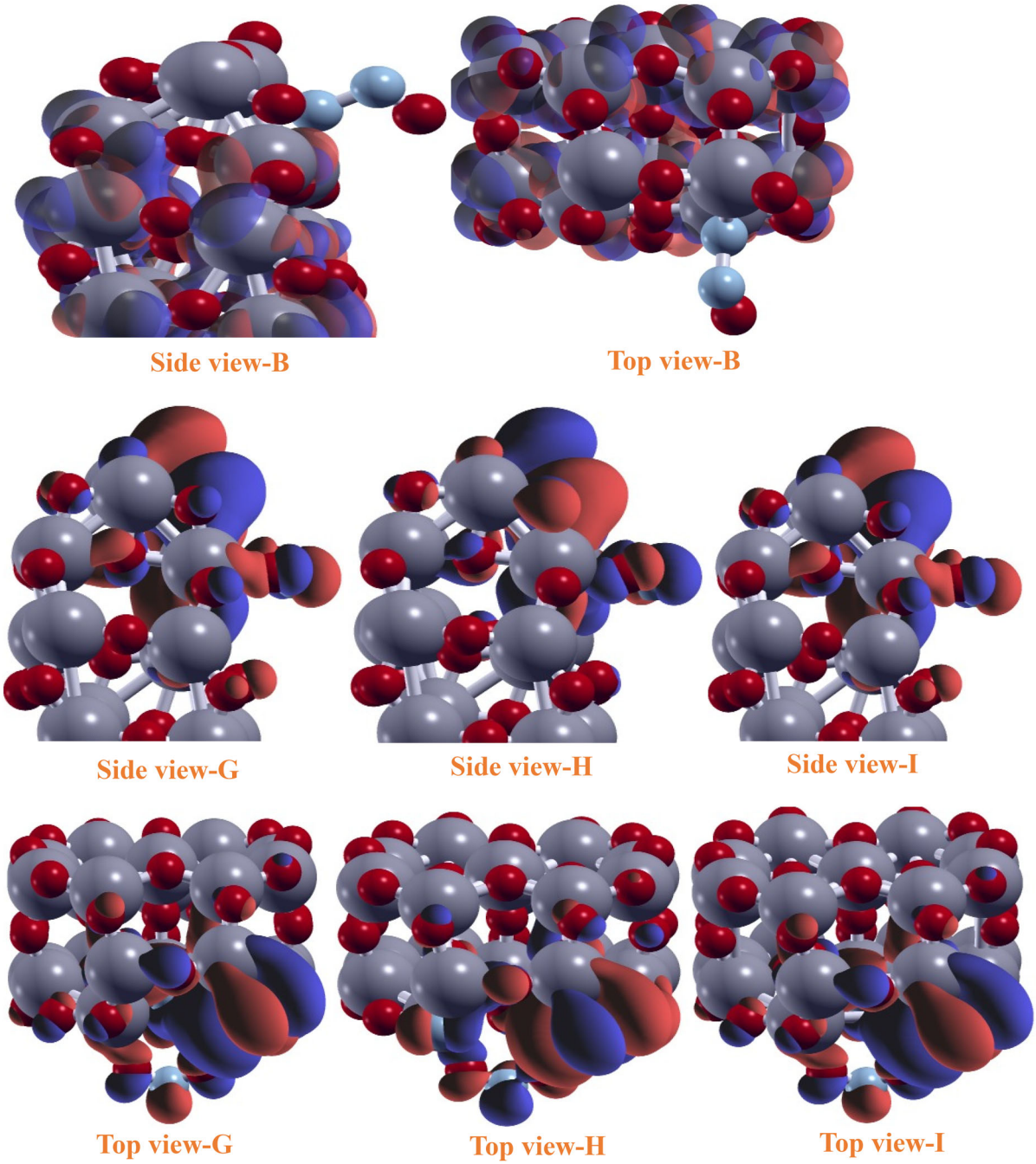

Fig. 16 Isosurfaces of HOMO molecular orbitals for the adsorption of NO and NO_2 molecules on the TiO_2/MoS_2 nanocomposites, where |0.05| was used as an isovalue of the molecular orbital

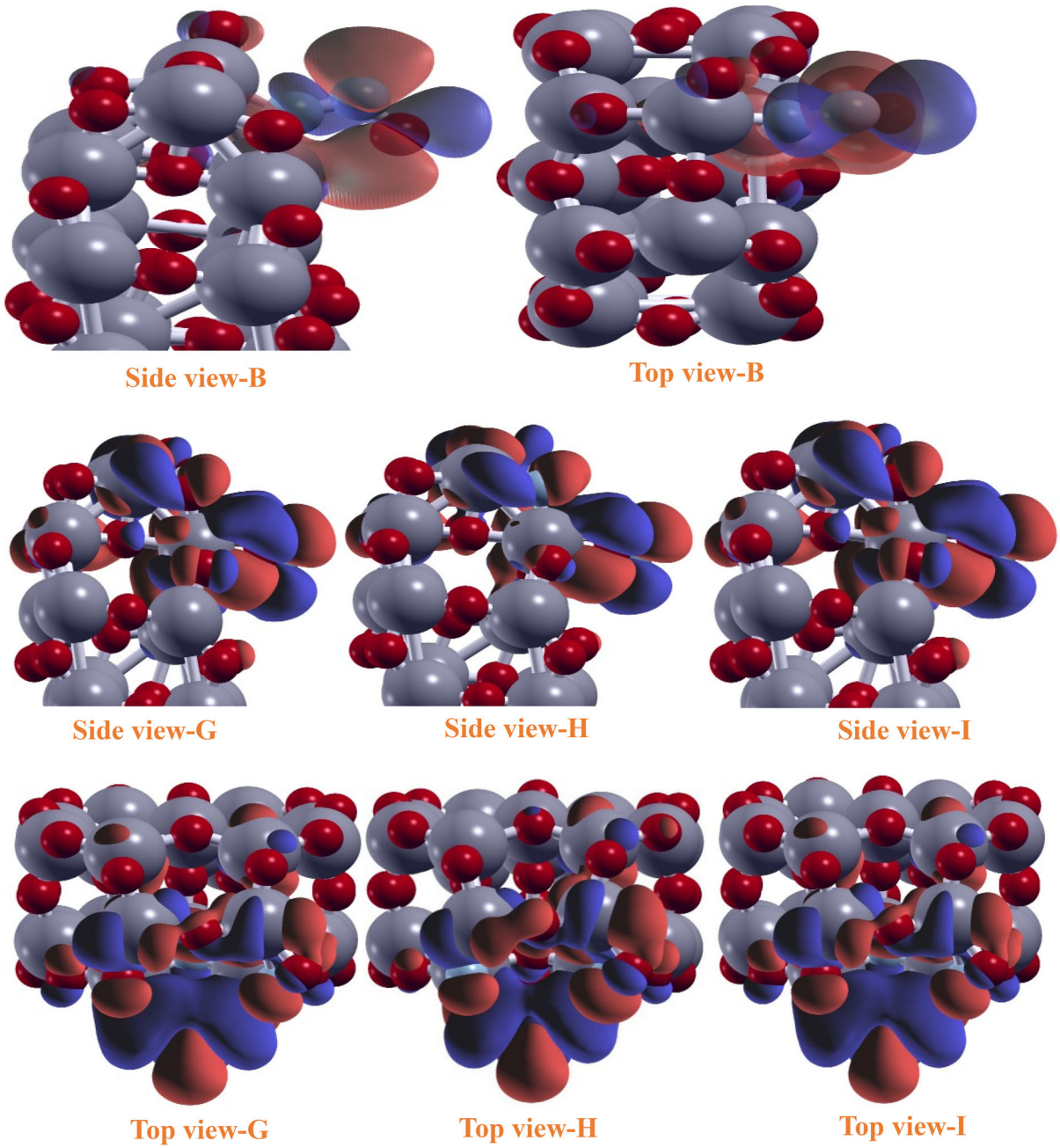

Fig. 17 Isosurfaces of LUMO molecular orbitals for the adsorption of NO and NO_2 molecules on the TiO_2/MoS_2 nanocomposites, where |0.05| was used as an isovalue of the molecular orbital

results also suggest that the N-doped nanocomposites have a higher efficiency to interact with harmful NO_x molecules in the environment. In other words, the doping of nitrogen atom provides an increased affinity for the TiO_2/MoS_2 nanocomposites to interact with NO_x molecules. The analysis of adsorption energies reveals that the adsorption of NO_x molecules on the N-doped TiO_2/MoS_2 nanocomposites is more favorable in energy than the adsorption of NO_x on the undoped ones. The variation in the electronic structure and molecular orbitals induced by N-doping is found to be responsible for the conductivity of the nanocomposite system. Our calculated results, therefore, suggest a theoretical basis for the prospective application of TiO_2/MoS_2 hybrid nanostructures as gas sensors for important air pollutants, such as NO and NO_2, in the environment.

Acknowledgments This work was supported by Azarbaijan Shahid Madani University [217/D/14271].

References

1. Fujishima, A., Zhang, X., Tryk, D.A.: TiO_2 photocatalysis and related surface phenomena. J. Surf. Sci. Rep. **63**, 515–582 (2008)
2. Fernandez-Garcia, M., Martinez-Arias, A., Hanson, J.C., Rodriguez, J.A.: Nanostructured oxides in chemistry: characterization and properties. J. Chem. Rev. **104**, 4063–4104 (2004)
3. Tang, S., Cao, Z.: Adsorption of nitrogen oxides on graphene and graphene oxides: insights from density functional calculations. J. Chem. Phys. **134**, 044710 (1-14) (2011)
4. Tang., S, Zhu, J.: Structural and electronic properties of Pd decorated graphene oxides and their effects on the adsorption of nitrogen oxides: insights from density functional calculations. J. RSC Adv. **4**, 23084–23096 (2014)
5. Topalian, Z., Niklasson, G.A., Granqvist, C.G., Österlund, L.: Spectroscopic study of the photofixation of SO_2 on anatase TiO_2 thin films and their oleophobic properties. ACS Appl. Mater. Interf. **4**, 672–679 (2012)
6. Li, W.K., Gong, X.Q., Lu, G., Selloni, A.: Different reactivities of TiO_2 polymorphs: comparative DFT calculations of water and formic acid adsorption at anatase and brookite TiO_2 surfaces. J. Phys. Chem. C **112**(17), 6594–6596 (2008)
7. Nambu, A., Graciani, J., Rodriguez, J.A., Wu, Q., Fujita, E., Sanz, J.F.: N doping of TiO_2 (110) Photoemission and density-functional studies. J. Chem. Phys. **125**, 094706(1–8) (2006)
8. Rumaiz, A.K., Woicik, J.C., Cockayne, E., Lin, H.Y., Jaffari, G.H., Shah, S.I.: Oxygen vacancies in N doped anatase TiO_2: experiment and first-principles calculations. J. Appl. Phys. Lett. **95**(26), 262111 (1–3) (2009)
9. Liu, D., Chen, X., Li, D., Wang, F., Luo, X., Yang, B.: Simulation of MoS_2 crystal structure and the experimental study of thermal decomposition. J. Mol. Struct. **980**, 66–71 (2010)
10. Wang, H., Yu, L., Lee, Y.H., Shi, Y., Hsu, A., Chin, M.L., Li, L.J., Dubey, M., Kong, J., Palacios, T.: Integrated circuits based on bilayer MoS_2 transistors. Nano Lett. **12**, 4674–4680 (2012)
11. Kou, L., Tang, C., Zhang, Y., Heine, T., Chen, C., Frauenheim, T.: Tuning magnetism and electronic phase transitions by strain and electric field in Zigzag MoS2 nanoribbons. J. Phys. Chem. Letts. **3**, 2934–2941 (2012)
12. Bertolazzi, S., Brivio, J., Kis, A.: Stretching and breaking of ultrathin MoS_2. ACS Nano **5**(12), 9703–9709 (2011)
13. Dolui, K., Pemmaraju, C.D., Sanvito, S.: Electric field effects on armchair MoS_2 nanoribbons. ACS Nano **6**(6), 4823–4834 (2012)
14. Yang, S., Li, D., Zhang, T., Tao, Z., Chen, J.: First-principles study of zigzag MoS_2 nanoribbon as a promising cathode material for rechargeable Mg batteries. J. Phys. Chem. C **116**, 1307–1312 (2012)
15. Frame, F.A., Osterloh, F.E.: CdSe-MoS_2: a quantum size-confined p CdSe-MoS_2: a quantum size-confined photocatalyst for hydrogen evolution from water under visible light. J. Phys. Chem. C **114**, 10628–10633 (2010)
16. Li, T.S., Galli, G.L.: Electronic properties of MoS2 nanoparticles. J. Phys. Chem. C **111**, 16192–16196 (2007)
17. Radisavljevic, B., Radenovic, A., Brivio, J., Giacometti, V., Kis, A.: Single-layer MoS2 transistors. Nat. Nanotechnol. **6**, 147–150 (2011)
18. Lembke, D., Kis, A.: Breakdown of high-performance monolayer MoS_2 transistors. ACS Nano **6**, 10070–10075 (2012)
19. Li, H., Yin, Z., He, Q., Li, H, Huang, X., Lu, G., Fam, D.W.H., Tok, A.I.Y., Zhang, H.: Fabrication of single-and multilayer MoS2 film-based field-effect transistors for sensing NO at room temperature. Small. **8**(1), 63–67 (2012)
20. He, Q., Zeng, Z., Yin, Z., Li, H., Wu, S., Huang, X., Zhang, H.: Fabrication of flexible MoS2 thin-film transistor arrays for practical gas-sensing applications. Small **8**(19), 2994–2999 (2012)
21. Liu, H., Neal, A.T., Ye, P.D.: Channel length scaling of MoS_2 MOSFETs. ACS Nano **6**, 8563–8569 (2012)
22. Zhou, W., Yin, Z., Du, Y., Huang, X., Zeng, Z., Fan, Z., Liu, H., Wang, J., Zhang, H.: Synthesis of few-layer MoS2 nanosheet-coated TiO2 nanobelt heterostructures for enhanced photocatalytic activities. Small **9**(1), 140–147 (2013)
23. Hu, K.H., Hu, X.G., Xu, Y.F., Sun, J.D.: Synthesis of nano-MoS_2/TiO_2 composite and its catalytic degradation effect on methyl orange. J. Mater. Sci. **45**(10), 2640–2648 (2010)
24. Shokuhi-Rad, A., Esfahanian, M., Maleki, S., Gharati, G.: Application of carbon nanostructures toward SO_2 and SO_3 adsorption: a comparison between pristine graphene and N-doped graphene by DFT calculations. J. Sulfur Chem. **37**(2), 176–188 (2016)
25. Hohenberg, P., Kohn, W.: Inhomogeneous electron gas. J. Phys. Rev. **136**, B864–B871 (1964)
26. Kohn, W., Sham, L.: Self-consistent equations including exchange and correlation effects. J. Phys. Rev. **140**, A1133–A1138 (1965)
27. Ozaki, T., Kino, H., Yu, J., Han, M.J., Kobayashi, N., Ohfuti, M., Ishii, F., et al.: User's manual of OPENMX version 3.8. http://www.openmxsquare.org
28. Ozaki, T., Kino, H.: Numerical atomic basis orbitals from H to Kr. J. Phys. Rev. B. **69**(1–19), 195113 (2004)
29. Ozaki, T., Kino, H.: Variationally optimized basis orbitals for biological molecules. J. Phys. Rev. B. **121**(22), 10879–10888 (2005)
30. Perdew, J.P., Burke, K., Ernzerhof, M.: Generalized gradient approximation made simple. J. Phys. Rev. Lett. **78**, 1396 (1997)
31. Koklj, A.: Computer graphics and graphical user interfaces as tools in simulations of matter at the atomic scale. J Comput Mater Sci. **28**, 155–168 (2003)
32. Schneider, W.F.: Qualitative differences in the adsorption chemistry of acidic (CO_2, SO_x) and amphiphilic (NO_x) species on the alkaline earth oxides. J. Phys. Chem. B. **108**, 273–282 (2004)
33. Liu, Q., Li, L., Li, Y., Gao, Z., Chen, Z., Lu, J.: Tuning electronic structure of bilayer MoS_2 by vertical electric field: a first-principles investigation. J. Phys. Chem. C **116**, 21556–21562 (2012)
34. Li, Y., Zhou, Z., Zhang, S., Chen, Z.: MoS_2 nanoribbons: high stability and unusual electronic and magnetic properties. J. Am. Chem. Sci. **130**(49), 16739–16744 (2012)
35. Pan, H., Zhang, Y.W.: Tuning the electronic and magnetic properties of MoS2 nanoribbons by strain engineering. J. Phys. Chem. C **116**, 11752–11757 (2012)
36. Web page at: http://rruff.geo.arizona.edu/AMS/amcsd.php
37. Wyckoff, R.W.G.: Crystal structures. (2nd Eds.) Interscience Publishers, USA (1963)
38. Wu, C., Chen, M., Skelton, A.A., Cummings, P.T., Zheng, T.: Adsorption of arginine–glycine–aspartate tripeptide onto negatively charged rutile (110) mediated by cations: the effect of surface hydroxylation. ACS Appl. Mater. Interf. **5**, 2567–2579 (2013)